Large format, Broadband and Multi-Color GaAs/AlGaAs Quantum Well Infrared Photodetector (QWIP) Focal Plane Arrays

S. V. Bandara, S. D. Gunapala, J. K. Liu, S. B. Rafol, D. Z. Ting, J. M. Mumolo, F. M. Reininger, J. M. Fastenau*, and A. K. Liu*

Jet Propulsion Laboratory, California Institute of Technology
4800, Oak Grove Drive, Pasadena, CA 91109
* IQE Inc., 119 Technology Drive, Bethlehem, PA 18015

ABSTRACT

The GaAs/AlGaAs based Quantum Well Infrared Photodetectors (QWIPs) afford greater flexibility than the usual extrinsically doped semiconductor IR detectors because the wavelength of the peak response and cutoff can be continuously tailored over any wavelength between 6-20 μm. The spectral band width of these detectors can be tuned from narrow ($\Delta\lambda/\lambda$ ~ 10 %) to wide ($\Delta\lambda/\lambda$ ~ 50 %) allowing various applications. Also, QWIP offers multi-color infrared cameras which is capable of simultaneously acquiring images in different infrared bands. Each pixel of such array consists of vertically stacked, independently readable, QWIP detectors sensitive in different narrow ($\Delta\lambda$ ~ 1 μm) infrared bands. In this article, we discuss the results of a 10-16 μm large format broadband QWIP focal plane array (FPA). The size of the FPA is 640x512 and its pixel pitch is 25 microns. The highest operating temperature of the FPA is 45K, and it was determined by the charge storage capacity and the other features of the particular readout multiplexer used in this demonstration. Excellent imagery, with a noise equivalent differential temperature (NEΔT) of 55 mK has been achieved. In addition, we will discuss the developments and results of the 640x512 dual-band QWIP FPA.

Keywords: Broadband, Multi-band, Intersubband Transitions, Infrared (IR), Long-wavelength Infrared (LWIR), Very Long-wavelength (VLWIR), Gallium Arsenide (GaAs), Quantum Well Infrared Photodetector (QWIP), Focal Plane Arrays, Infrared Imaging

1. INTRODUCTION

Long Wavelength Infrared (LWIR) staring focal plane arrays (FPAs) play critical roles in many defense applications as well as NASA's earth science, space-science and human exploration applications. The vast majority of applications are in 6-16 micron infrared band because photons in this band can excite rotational and vibrational modes of various species of gas molecules generating absorption and emission bands in the infrared spectrum. In additional, tactical missions usually require FPAs operating in the atmospheric LWIR window (8-12 μm). Large format, staring FPAs have obvious advantages over the earlier generations of linear scanning arrays because they focus on an entire wide field of view uninterruptedly which gives them a much longer integration time. Together with the high uniformaty and high stability, the focal plane give the sensor system much higher resolution and greater system sensitivity which translate into a better image with higher noise equivalent temperature difference (NEDT). Staring arrays also simplifies the whole sensor system by eliminating the scanning mechanism, related electronics and reducing the complexity.

In recent years, quantum well infrared photodetectors (QWIPs) have shown remarkable progress in LWIR imaging with highly uniform large format FPAs [1-4]. Fabricated entirely from large bandgap materials which are easy to grow and process, it is now possible to obtain large format highly uniform FPAs of QWIPs tuned to detect light at wavelengths from 6 to 25 μm in the GaAs/Al_xGa_{1-x} As material system [5-7]. As a result of matured fabrication and processing technologies of the materials used, this breakthrough new technology has already demonstrated large format FPAs with high unifomity, high operability, high stability (low 1/f noise), and higher yield [5-9]. In addition,

high radiation tolerance is expected in QWIPs in contrast to narrow bandgap semiconductor detectors due to the use of larger bandgap material such as GaAs/AlGaAs. These properties will enable in longer science missions with lower operating costs. Typically, QWIPs are fabricated out of eptiaxially grown III-V alloy layers (GaAs, $Al_xGa_{1-x}As$ and $Ga_yIn_{1-y}As$) on 3" GaAs wafers (now 4" and 6" wafers are available) [3-5] JPL has already demonstrated a 8-9 μm 640x486 QWIP camera with 22 μm pixel size [4]. These results show that an extension of the development to larger formats should be straightforward and relatively low risk. As a result of advance substrate removal process, QWIP large format FPAs are completely immune to thermal mismatch problems between silicon CMOS readout and GaAs based QWIP array, temperature cycling effects, and pixel delamination. In addition, high yield in fabrication and reproducibility of this technology will result in a lower cost for detector arrays than competing technologies.

2. BROADBAND QWIP

Unlike the responsivity spectrums of intrinsic infrared detectors, the responsivity spectrums of QWIPs are much narrower and sharper due to their resonance intersubband absorption [6,7]. Recently, we have developed a technique to design a broad-band QWIP by replacing single quantum wells with small superlattice structures (several quantum wells separated by thin barriers) in the multi-quantum well structure [8]. Such a scheme creates an excited state miniband due to overlap of the excited state wavefunctions of quantum wells. Energy band calculations based on a two band model shows excited state energy levels spreading greater than 30 meV [8]. The spectral band width of these detectors can be tuned from narrow ($\Delta\lambda/\lambda$ ~ 10 %) to wide ($\Delta\lambda/\lambda$ ~ 50 %) allowing various applications. Thus, control of the processing allows us to tailor the QWIP characteristics tuned from narrow ($\Delta\lambda/\lambda$ ~ 10 %) to wide ($\Delta\lambda/\lambda$ ~ 50 %) in 6-20 μm spectral band allowing various applications

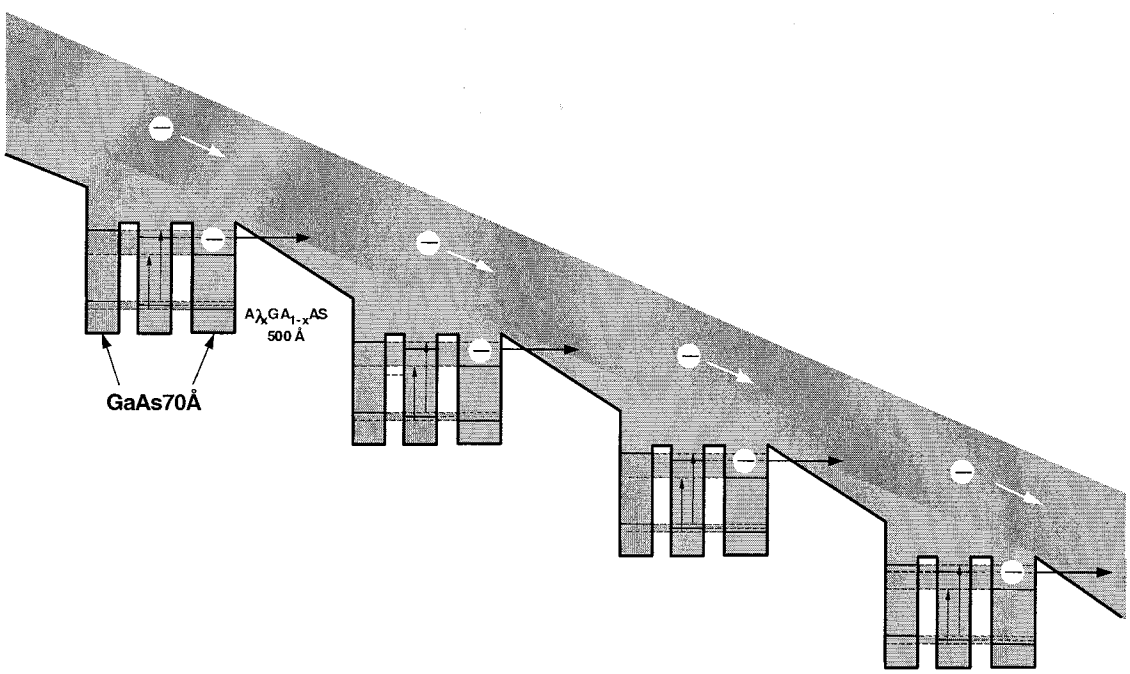

Fig. 1. Broad-band MQW structure is designed by repeating a unit of several quantum wells with slightly different parameters such as well width and barrier height. The excited state energy levels broadened due to overlap of the wavefunctions associated with excited states of quantum wells separated by thin barriers.

As shown in Fig 1, the MQW structure consists of many periods of these three-quantum-well units separated by thick barriers. The device structure reported here involved 33 repeated layers of GaAs three-quantum-well units

separated by L_B ~ 575 Å thick $Al_xGa_{1-x}As$ barriers (See Fig 1). The well thickness of the quantum wells (see Fig. 1) of three-quantum-well units are designed to respond at peak wavelengths around 13, 14, and 15μm respectively. The positions of ground and excited states of the quantum well are determined by the quantum well width (L_w) and the barrier height , i.e. the Al mole fraction (x) of the barrier [6,7]. Since each single set of parameters for a bound-to-quasibound quantum well [9] corresponds to a spectral band pass of about 1.5 μm, three different sets of values are sufficient to cover a 10-16 μm spectral region. These wells are separated by L_u ~ 75 Å thick $Al_xGa_{1-x}As$ barriers. The Al mole fraction (x) of barriers throughout the structure was chosen such that the λ_p = 13 μm quantum well operates under bound-to-quasibound conditions [9]. The sample was grown on a semi-insulating 3-inch GaAs substrate by molecular beam epitaxy. It consists of the device structure described above sandwiched between top and bottom contact layers. Transport carriers (electrons) were provided by doping all GaAs wells and contact layers with Si. In order to measure dark current-temperature curve, spectral responsivity and noise, 200 μm diameter mesas were fabricated using wet chemical etching and Au/Ge ohmic contacts were evaporated onto the top and bottom contact layers.

The responsivity spectra of these detectors were measured using a 1000 K blackbody source and a grating monochromator. The detectors were back illuminated through a 45° polished facet to obtain normalized responsivity spectra at different bias voltages. Then the absolute spectral responsivities were obtained by measuring total photocurrent from a calibrated black-body source. In Fig. 2, responsivity curve at V_B = -2.5 V bias voltage shows broadening of the spectral response up to $\Delta\lambda$ ~ 5.5 μm, i.e. the full width at half maximum from 10.5 - 16μm. This broadening $\Delta\lambda/\lambda_p$ ~ 42 % is about a 400 % increase compared to a typical bound-to-quasibound QWIP [8]. The responsivity of the detector peaks at 13.5 μm and the peak responsivity (R_p) of the detector is 250 mA/W at bias V_B = -2.5 V. The bias dependent peak responsivity of the detector is shown in Fig. 3. The measured absolute peak responsivity of the detector is small, up to about V_B = -0.5 V. Beyond that it increases nearly linearly with bias reaching R_P = 580 mA/W at V_B = -3.5 V. This type of behavior of responsivity versus bias is typical for a bound-to-quasibound QWIP. The peak quantum efficiency was 11% at bias V_B = -2.5 V for a 45° double pass. The lower quantum efficiency is due to the lower well doping density ($2x10^{17}$ cm^{-3}) as it is necessary to suppress the dark current at the highest possible operating temperature. A peak quantum efficiency as high as 25% has already been achieved with regular well doping density (i.e., $1x10^{18}$ cm^{-3}). Due to lower readout multiplexer well depth (i.e., $11x10^6$ electrons) a lower dark current is mandatory to achieve a higher operating temperature. In this case, the highest operating temperature of 45 K was determined by the well depth of the readout multiplexer.

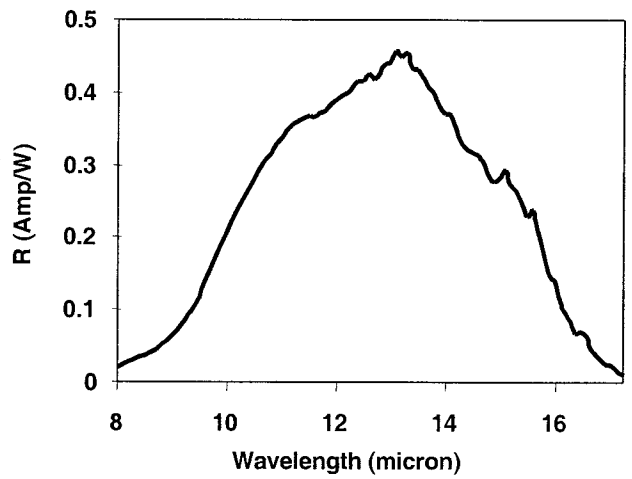

Fig. 2 Responsivity spectrum of a broadband QWIP test structure at temperature T = 55 K. The spectral response peak is at 13.5 μm and the long wavelength cutoff is at 15.4 μm.

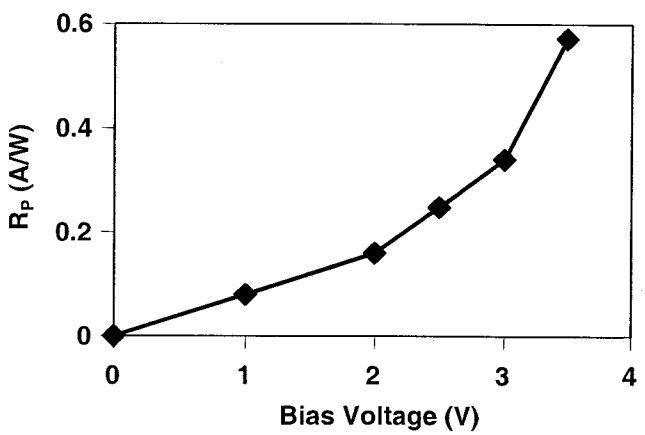

Fig. 3. *Peak responsivity as a function of bias voltage at temperature T = 55 K.*

The dark current noise i_n of the device was measured using a spectrum analyzer at T = 55 K as a function of bias voltage. The noise gain g_n can now be obtained using the g-r noise calculated based on standard noise expression: $i_n = \sqrt{4eI_d g_n \Delta B}$ where I_d is the dark current and ΔB is the band width. Using experimental measurements of noise and responsivity, one can now calculate specific detectivity D^* form $D^* = R\sqrt{A\Delta f}\,/\,i_n$, where A is area of the detector. Calculated D* value for the present device (λ = 15.4 μm) at, T = 55 K, and V_B = 2.5 V is 3 x 10^{10} cm$\sqrt{Hz}$/W. Even with broader response, this D^* is comparable to previously reported D^* of QWIPs with narrow spectral response. Figures 4 and 5 show the detectivity D* and the noise equivalent temperature difference (NEΔT) as a function of the operating temperature of the device.

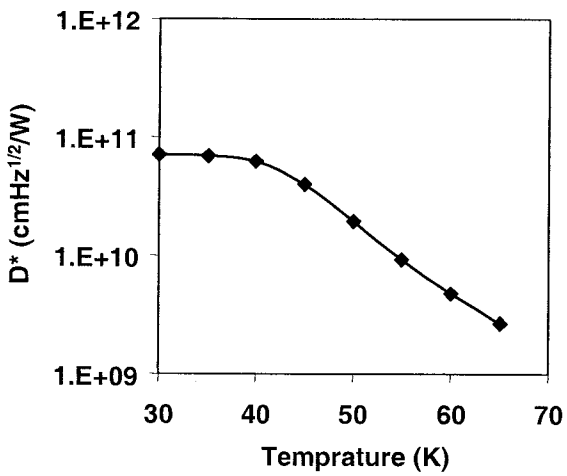

Fig. 5. Detectivity as a function of temperatures at bias voltage V_B = -2.5V.

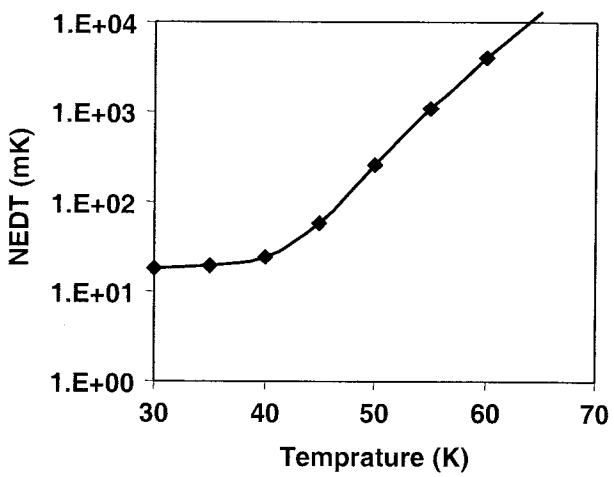

Fig. 5. Noise equivalent temperature difference as a function of temperatures at bias voltage V_B = -2.5V.

3. 640x512 BROADBAND QWIP FOCAL PLANE ARRAY

Figure 6 shows twelve processed QWIP FPAs on a 3-inch GaAs wafer. Indium bumps were then evaporated on top of the detectors for Si readout circuit (ROC) hybridization. A single QWIP FPA was chosen and hybridized (via indium bump-bonding process) to a 640x512 CMOS multiplexer (Indigo Systems 9803) and biased at V_B = -2.5 V (see figure 7). At temperatures below 48 K, the signal to noise ratio of the system is limited by array non-uniformity, multiplexer readout noise, and photo current (photon flux) noise. At temperatures above 48 K, temporal noise due to the QWIP's higher dark current becomes the limitation. As mentioned earlier this higher dark current is due to thermionic emission and thus causes the charge storage capacitors of the readout circuitry to saturate. Since the QWIP is a high impedance device, it should yield a very high charge injection coupling efficiency into the integration capacitor of the multiplexer [10].

The FPA was back- illuminated through the flat thinned substrate membrane (thickness ≈ 1300 Å). This thinned GaAs FPA membrane has completely eliminated the thermal mismatch between the silicon CMOS readout multiplexer and the GaAs based QWIP FPA. Thus, thinning has played an extremely important role in the fabrication of large area FPA hybrids. In addition, this thinning has completely eliminated the pixel-to-pixel optical cross-talk of the FPA. This initial array gave very good images with 99.9% of the pixels working, demonstrating the high yield of GaAs technology. The operability was defined as the percentage of pixels having noise equivalent differential temperature less than 100 mK at 300 K background with f/2 optics.

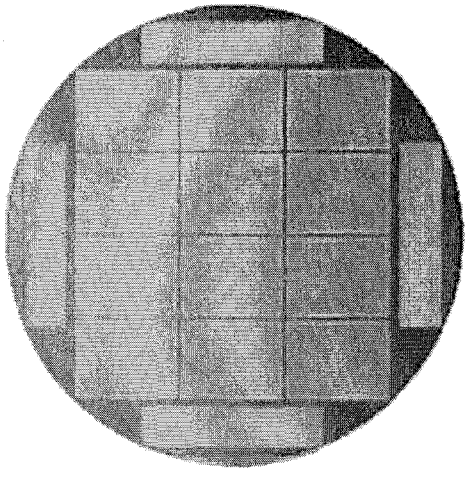

Fig. 6. Twelve 640x512 QWIP focal plane arrays on a 3 in. GaAs wafer.

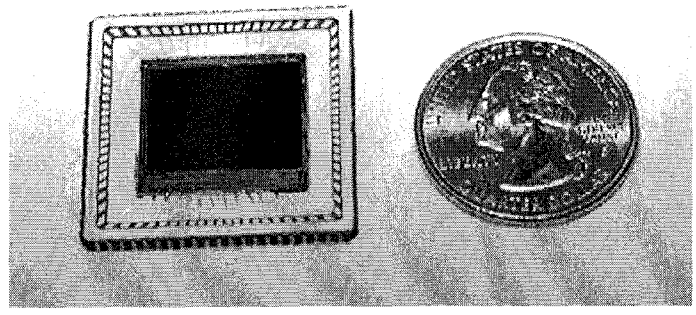

Fig. 7. A size comparison of the 640 x 512 long-wavelength QWIP FPA to a quarter.

4. IMAGERY WITH BROADBAND ARRAY

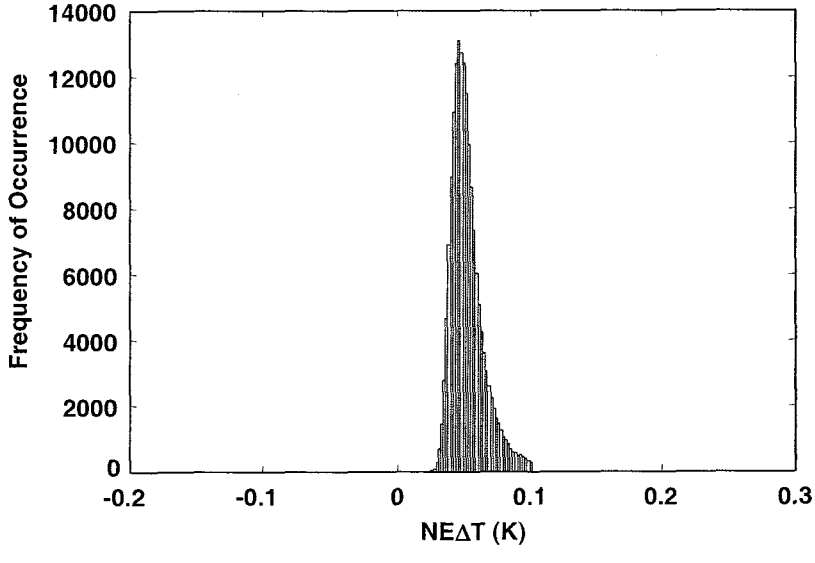

Fig. 8. Noise equivalent temperature difference (NEΔT) histogram of the 327,680 pixels of the 640 x 512 array showing a high uniformity of the FPA. The uncorrected non-uniformity (= standard deviation/mean) of this unoptimized FPA is only 6.3% including 1% non-uniformity of ROC and 1.4% non-uniformity due to the cold-stop not being able to give the same field of view to all the pixels in the FPA.

A 640X512 QWIP FPA hybrid was mounted onto a 84-pin lead-less chip carrier and installed into a laboratory dewar which is cooled by liquid neon to demonstrate a LWIR imaging camera (FPA was cooled to 35K). It is designed to be transparent in the 8-12 μm wavelength range (which is not fully compatible with the 10-15 micron broadband QWIP array). SEIR image processing station was used to obtain clock signals for readout multiplexer and to perform digital data acquisition and non-uniformity corrections. The digital data acquisition resolution of the camera is 14-bits, which determines the instantaneous dynamic range of the camera (i.e., 16,384), however, the dynamic range of QWIP is 85 Decibels.

The measured mean NEΔT of the QWIP camera is 55 mK at an operating temperature of T = 35 K and bias V_B = -2.5 V at 300 K background with f/2 optics. See Figure 8. This is in good agreement with expected focal plane array sensitivity due to the practical limitations on charge handling capacity of the multiplexer, read noise, bias voltage and operating temperature. The uncorrected NEΔT non-uniformity (which includes a 1% non-uniformity of the ROC and a 1.4% non-uniformity due to

the cold-stop in front of the FPA not yielding the same field of view to all the pixels) of the 327,680 pixels of the 640x512 FPA is about 6.3% (= sigma/ mean). The non-uniformity after two-point (17° and 27° Celsius) correction improves to an impressive 0.1%. As mentioned earlier, this high yield is due to the excellent GaAs growth uniformity and the mature GaAs processing technology.

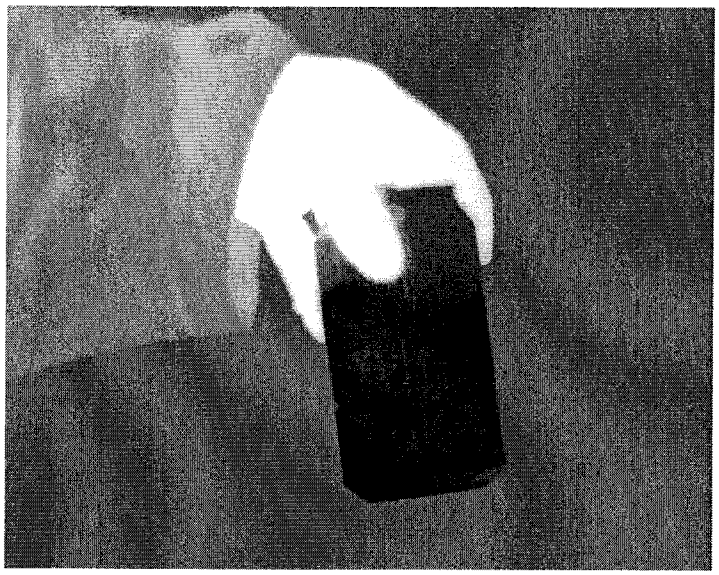

Fig. 9. This picture shows a frame of video image taken with this 10-15.4 mm 640x512 broadband QWIP imager. This image shows the liquide level of the soda can and some finger prints on the can.

Video images were taken at a frame rate of 15 Hz at temperatures as high as T = 35 K using a ROC capacitor having a charge capacity of $11x10^6$ electrons (the maximum number of photoelectrons and dark electrons that can be counted in the integration time of each detector pixel). Figure 9 shows a frame of video image taken with this 10-15.4 mm 640x512 broadband QWIP imager. These high resolution images comparable to standard TV, demonstrate the high operability (i.e., 99.9%) and the stability (i.e., lower residual uniformity and 1/f noise) of the 640 x 512 long-wavelength QWIP staring array camera. It should be noted that these initial unoptimized FPA results are far from optimum. The light coupling gratings were not optimized (as described earlier) for maximum light coupling efficiency, no anti-reflection coatings were used on the backside of the FPA.

5. MULTI COLOR QWIPs

Due to the inherent properties such as narrow-band response, wavelength tailorability, and stability (i.e., low 1/f noise) associated with GaAs based QWIPs [6-8], it is an ideal candidate for large format long-wavelength multi-color FPAs. The LWIR and VLWIR dualband QWIP device structure described in this section can be processed into interlace readable dualband FPA (i.e., odd rows for one color and the even rows for the other color) [4]. This scheme are that it provides simultaneous data acquisition and allows the use of currently available single color CMOS readout multiplexers. However, the disadvantage is that it does not provide a full fill factor for both wavelength bands.

The device structure consists of a 30 period stack, of VLWIR QWIP structure and a 18 periods stack of LWIR QWIP structure separated by a heavily doped 0.5 μm thick intermediate GaAs contact layer (see Figure 10). The first stack (VLWIR) consists of 30 periods of a 500 Å $Al_xGa_{1-x}As$ barrier and a 60 Å GaAs well. Since the dark current of this device structure is dominated by the longer wavelength portion of the device structure, the VLWIR QWIP structure has been designed to have a bound-to-quasibound intersubband absorption peak at 14.5 μm. The second stack (LWIR) consists of 18 periods of a 500 Å $Al_xGa_{1-x}As$ barrier and a narrow 40 Å GaAs well. This LWIR QWIP structure has been designed to have a bound-to-continuum intersubband absorption peak at 8.5 μm, because the photo current and dark current of the LWIR device structure is relatively small compared to the VLWIR portion of the device structure. This whole dualband QWIP structure is then sandwiched between 0.5 μm GaAs top and bottom contact layers doped with n = 5×10^{17} cm^{-3}, and was grown on a semi-insulating GaAs substrate by MBE. A 300 Å $Al_{0.3}Ga_{0.7}As$ stop-etch layer and a 1.0 μm thick GaAs cap layer were then grown in situ on top of the device structure. GaAs wells of the LWIR and VLWIR stacks were doped with n = $6x10^{17}$ and $2.5x10^{17}$ cm^{-3}, respectively. All contact layers were doped to n = $5x10^{17}$ cm^{-3}. The GaAs well doping density of the LWIR stack was intentionally increased by a factor of two to compensate for the reduced number of quantum wells in the LWIR stack. It is worth noting that, the total (dark current + photo current)

current of each stack can be independently controlled by carefully designing the position of the upper state, well doping densities, and the number of periods in each MQW stack. All of these features were utilized to obtain approximately equal total currents from each MQW stack.

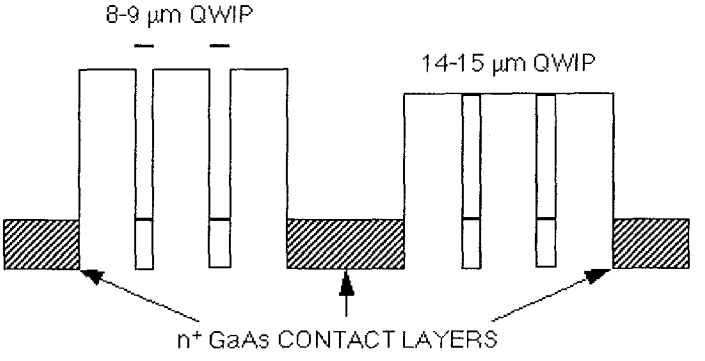

Fig. 10 Conduction band energy diagram of the long-wavelength and very long-wavelength two-color infrared detector. The long-wavelength (8-9 μm) sensitive MQW stack utilizes the bound-to-continuum intersubband absorption. The very long-wavelength (14-15 μm) sensitive MQW stack utilizes the bound-to-quasibound intersubband absorption

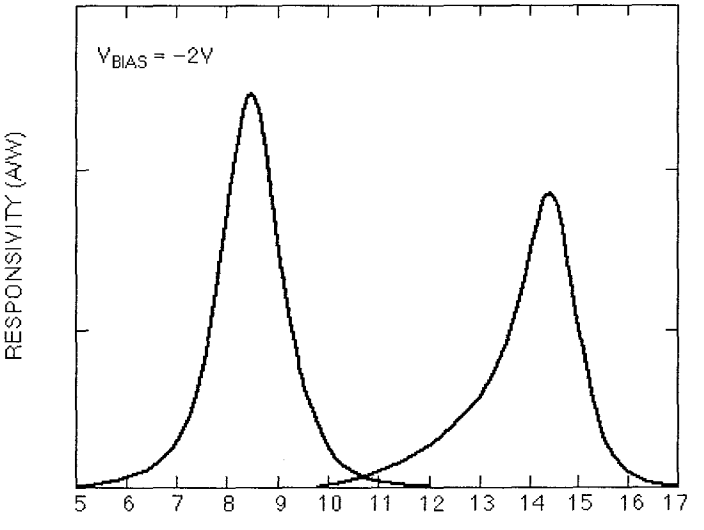

Fig. 11 Simultaneously measured responsivity spectrum of vertically integrated LWIR and VLWIR dualband QWIP detector (45 degree illumination).

The simultaneously measured responsivity spectra of these vertically integrated dualband QWIPs are shown in Figure 11. The responsivity of the LWIR detectors peaks at 8.4 μm and the peak responsivity (R_p) of the detector is 509 mA/W at bias V_B = -2 V. The spectral width and the cutoff wavelength of the LWIR detectors are $\Delta\lambda/\lambda$ = 16% and λ_c = 9.1 μm, respectively. The responsivity of the VLWIR detectors peaks at 14.4 μm and the peak responsivity (R_p) of the detector is 382 mA/W at bias V_B = -2.0 V. The spectral width and the cutoff wavelength of the VLWIR detector are $\Delta\lambda/\lambda$ = 10% and λ_c = 15 μm, respectively. The measured absolute peak responsivity of both LWIR and VLWIR detectors is small, up to about V_B = -0.5 V. Beyond that, it increases almost linearly with bias in both LWIR and VLWIR detectors reaching R_P = 0.3 (at V_B = -2V) and 1 A/W (at V_B = -3V), respectively. This behavior of responsivity versus bias is typical for bound-to-continuum and bound-to-quasibound QWIPs in LWIR and VLWIR bands respectively. The peak absorption quantum efficiencies of LWIR and VLWIR detectors operating at bias V_B=-2 V were 6.4% and 11.6%, respectively. Based on single element test detector data, the LWIR detectors show background limited performance (BLIP) at bias V_B = -2 V and temperature T = 72 K for a 300 K background with f/2 cold stop. The VLWIR detectors reached BLIP under the same operating conditions at 45 K operating temperature.

Two different 2-D periodic grating structures were designed to independently couple the 8-9 and 14-15 μm radiation into the detector pixels of even and odd rows of the FPAs. The top 0.7 μm thick GaAs cap layer was used to fabricate the light coupling 2-D periodic grating for 8-9 μm detector pixels. The light coupling for 2-D periodic gratings of the 14-15 μm detector pixels were fabricated through the photosensitive LWIR MQW layers. This grating scheme short circuited all 8-9 μm sensitive detectors in all the odd rows of the FPAs. Thus, the total thickness of 8-9 μm detector is limited by the grating layer thickness of the VLWIR detector. This 2-D periodic grating structure is fabricated on the detectors by using standard photolithography and SF_6:BCl_3 selective dry etching. Te detailed dual band FPA fabrication process is described elsewhere [4].

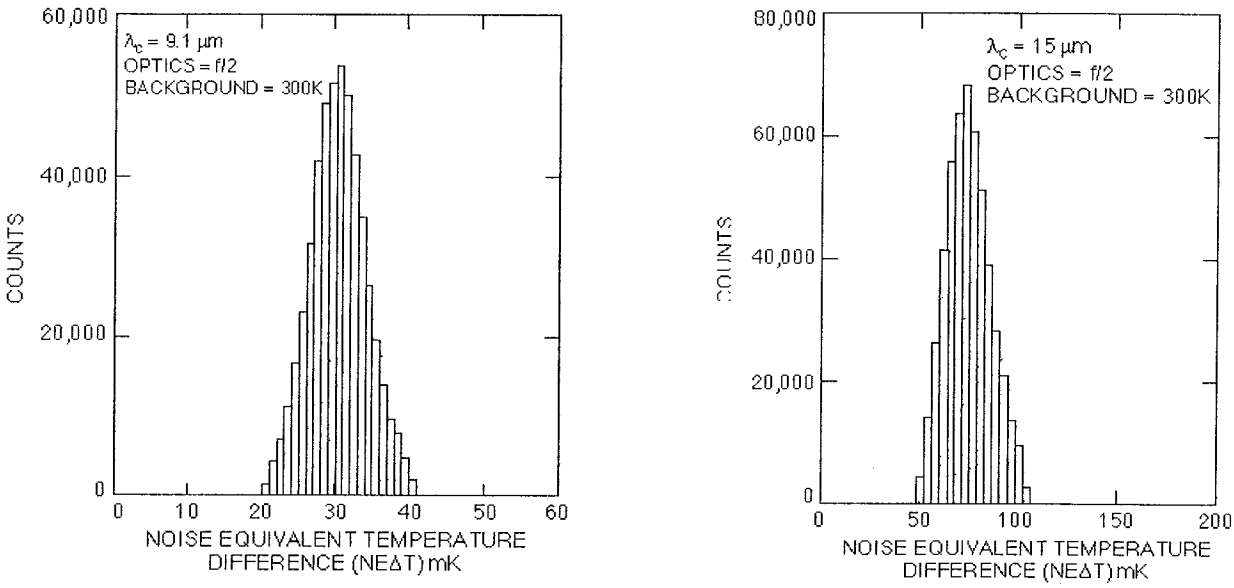

(a) (b)

Fig. 12 (a) The uncorrected noise equivalent temperature difference (NEΔT) histogram of 8-9 μm detector pixels of the 640x486 dualband FPA. The mean NEΔT is 29 mK. (b) The uncorrected NEΔT histogram of 14-15 μm detector pixels of the 640x486 dualband FPA. The mean NEΔT is 74 mK.

6. 640X512 DUAL BAND QWIP FPA

These dualband FPAs were tested at a background temperature of 300 K, with f/2 cold stop, and at 30 Hz frame rate. As expected (due to BLIP), the estimated and experimentally obtained NEΔT values of the LWIR detectors do not change significantly at temperatures below 65 K. The estimated NEΔT of LWIR and VLWIR detectors at 40 K are 36 and 44 mK, respectively (see Figures 12). These estimated NEΔT values based on the test detector data agree reasonably well with the experimentally obtained values. A dualband FPA hybrid was mounted onto the cold finger of a liquid helium cooled laboratory dewar, to demonstrate simultaneous dualband imagery at 8.5 and 14.5 μm. The camera is equipped with a 100 mm focal length f/2 germanium lens designed to be transparent in the 8-15 μm wavelength range, for compatibility with the 8-9 and 14-15 μm dualband operation. Due to transmission properties of germanium, the 14-15 μm band has only 30% transmission. This poor optical transmission has clearly affected the VLWIR performance and image quality. The operability of 8-9 μm detector pixels is 99.7% and the operability of 14-15 μm detector pixels is 98%. Video images were taken at a frame rate of 30 Hz and Figure 13 shows simultaneously acquired 8-9 and 14-15 micron images using this two-color (LWIR and VLWIR) imaging camera. Figure 14 shows a simultaneously acquired image of a filter pattern used to test the operating wavelengths of the two-color camera. The arrow and the semi-circle are open, and transmit all wavelengths. The diamond shape opening is covered with a 10 micron high-pass filter and the rectangle shape opening is covered with a 10 micron low-pass filter. This clearly verifies the 8-9 and 14-15 micron two-color operation of this dualband QWIP camera.

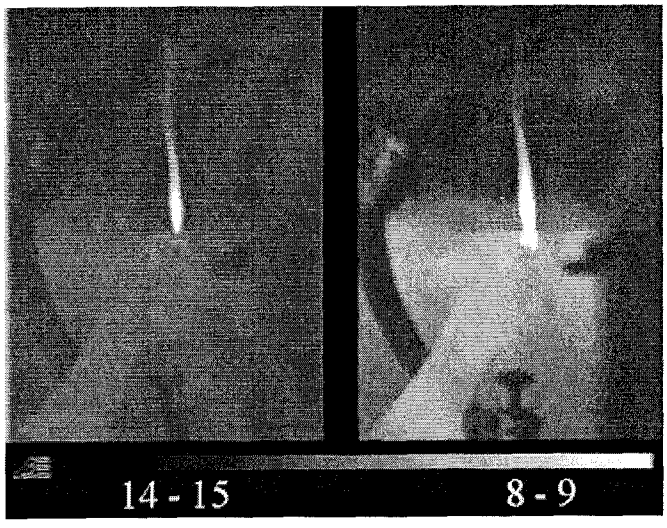

Fig. 13 Both pictures show (Flame - simultaneously acquired) two-color images with the 640x486 two-color QWIP camera. Image on the left is from 14-15 micron infrared and the image on the right is from 8-9 micron infrared. Pixel pitch of the FPA is 25 micron. The 14-15 micron image is less sharp due to the diffraction limited spot size being larger than the pixel pitch of the FPA.

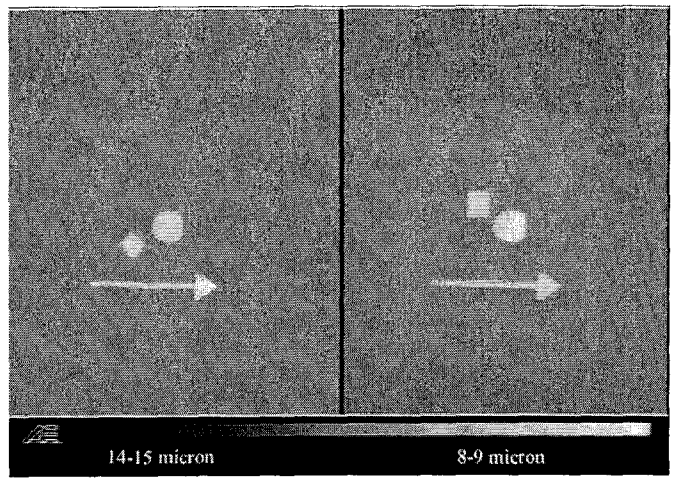

Fig. 14 A simultaneously acquired image of a filter pattern. The arrow and the semi-circle are open, and transmit all wavelengths. The diamond shape opening is covered with a 10 micron high-pass filter and the rectangle shape is covered with a 10 micron low-pass filter. This image clearly verifies the 8-9 and 14-15 micron two-color operation of this QWIP camera.

ACKNOWLEDGEMENT

The research described here was performed by the Center for Space Microelectronics Technology, Jet Propulsion Laboratory, California Institute of Technology, and was sponsored by the National Aeronautics and Space Administration, breakthrough sensor & instrument component technology thrust area of the cross enterprise technology development program.

REFERENCES

1. Sarath D. Gunapala, Jin S. Park, Gabby Sarusi, True-Lon. Lin, John K. Liu, Paul D. Maker, Richard E. Muller, Craig A. Shott, and Ted Hoelter, IEEE Trans. Electron Devices, 44, pp. 45-50, (1997).

2. Sarath D. Gunapala, John K. Liu, Jin S. Park, Mani Sundaram, Craig A. Shott, Ted Hoelter, True-Lon Lin, S. T. Massie, Paul D. Maker, Richard E. Muller, and Gabby Sarusi", IEEE Trans. Electron Devices, **44**, pp. 51-57 (1997).

3. S. D. Gunapala, S. V. Bandara, J. K. Liu, W. Hong, M. Sundaram, P. D. Maker, R. E. Muller, R. Carralejo, and C. A. Shott, IEEE Trans. Elec. Devices **45**, 1890 (1998).

4. S. D. Gunapala, S. V. Bandara, A. Singh, J. K. Liu, S. B. Rafol, E. M. Luong, J. M. Mumolo, N. Q. Tran, J. D. Vincent, C. A. Shott, J. Long, and P. D. LeVan, **47**, pp. 963-971, (2000).

5. S. D. Gunapala, S. V. Bandara, J. K. Liu, E. M. Luong, S. B. Rafol, J. M. Mumolo, D. Z. Ting, J. J. Bock, M. E. Ressler, M. W. Werner, P. D. LeVan, R. Chehayeb, C. A. Kukkonen, M. Levy, P. LeVan, and M. A. Fauci", Sensors and Materials, **12**, pp. 327-351, (2000).

6. S. D. Gunapala and S. V. Bandara, Physics of Thin Films, edited by M. H. Francombe, and J. L. Vossen, Vol. 21, pp. 113-237, Academic Press, NY, (1995).

7. S. D. Gunapala and S. V. Bandara, Quantum Well Infrared Photodetector (QWIP) Focal Plane Arrays, *Semiconductors and Semimetals*, 62, 197-282, Academic Press. (1999).

8. S. V. Bandara, S. D. Gunapala, J. K. Liu, E. M. Luong, J. M. Mumolo, W. Hong, D. K. Sengupta, and M. J. McKelvey, Appl. Phys. Lett. **72**, 2427 (1998).

9. S. D. Gunapala, J. K. Liu, J. S. Park, T. L. Lin, and M. Sundaram "INFRARED RADIATION DETECTING DEVICE", US Patent No. 6,211,529.

10. C. G. Bethea, B. F. Levine, M. T. Asom, R. E. Leibenguth, J. W. Stayt, K. G. Glogovsky, R. A. Morgan, J. D. Blackwell, and W. J. Parrish, IEEE Trans. Electron. Devices, **40**, pp. 1957-1963, (1993).